



OPEN

BODIPY nanoparticles functionalized with lactose for cancer-targeted and fluorescence imaging-guided photodynamic therapy

Duy Khuong Mai^{1,2,7}, Chanwoo Kim^{3,7}, Joomin Lee^{4,7}, Temmy Pegarro Vales⁵, Isabel Wen Badon¹, Koushitak De⁶, Sung Cho^{2✉}, Jaesung Yang^{3✉} & Ho-Joong Kim^{1✉}

A series of four lactose-modified BODIPY photosensitizers (PSs) with different substituents (-I, -H, -OCH₃, and -NO₂) in the *para*-phenyl moiety attached to the *meso*-position of the BODIPY core were synthesized; the photophysical properties and photodynamic anticancer activities of these sensitizers were investigated, focusing on the electronic properties of the different substituent groups. Compared to parent BODIPY H, iodine substitution (BODIPY I) enhanced the intersystem crossing (ISC) to produce singlet oxygen (¹O₂) due to the heavy atom effect, and maintained a high fluorescence quantum yield (Φ_F) of 0.45. Substitution with the electron-donating methoxy group (BODIPY OMe) results in a significant perturbation of occupied frontier molecular orbitals and consequently achieves higher ¹O₂ generation capability with a high Φ_F of 0.49, while substitution with the electron-withdrawing nitro group (BODIPY NO₂) led a perturbation of unoccupied frontier molecular orbitals and induces a forbidden dark S₁ state, which is negative for both fluorescence and ¹O₂ generation efficiencies. The BODIPY PSs formed water-soluble nanoparticles (NPs) functionalized with lactose as liver cancer-targeting ligands. BODIPY I and OMe NPs showed good fluorescence imaging and PDT activity against various tumor cells (HeLa and Huh-7 cells). Collectively, the BODIPY NPs demonstrated high ¹O₂ generation capability and Φ_F may create a new opportunity to develop useful imaging-guided PDT agents for tumor cells.

Photodynamic therapy (PDT) is a promising cancer treatment that has been applied to various cancers, such as oral, lung, bladder, brain, ovarian, and esophageal cancers^{1–3}. The PDT process requires three key components: light, oxygen, and a photosensitizing agent^{4,5}. In the presence of external light, the photosensitizer (PS) is photoexcited to the optically allowed S₁ state and then energetically relaxed to the T₁ state via intersystem crossing (ISC). The triplet excited PS can transfer the excitation energy to ground-state triplet oxygen (type II), resulting in cytotoxic reactive oxygen species (ROS), such as singlet oxygen (¹O₂), which directly kills tumor cells^{6–9}. PDT can provide good selectivity and is non-invasive at the treatment region as the activity of this medical technique is only carried out when the PS is combined with light of a particular wavelength¹⁰. Recently, imaging-guided PDT has been assessed to develop specific agents for visualizing individual tumor targets, thereby enhancing therapeutic efficiency and reducing side effects^{11–13}. However, to date, PSs that can be simultaneously applied for both imaging and treatment are not available in the clinic. Accordingly, there is an urgent need to develop PSs that can effectively produce both fluorescence and ROS^{14,15}.

¹Department of Chemistry, Chosun University, Gwangju 61452, Korea. ²Department of Chemistry, Chonnam National University, Gwangju 61186, Korea. ³Department of Chemistry, Yonsei University, Wonju 26493, Gangwon, Korea. ⁴College of Food and Nutrition, Chosun University, Gwangju 61452, Korea. ⁵Department of Natural Sciences, Caraga State University, 8600 Butuan City, Philippines. ⁶Department of Cellular and Molecular Medicine, College of Medicine, Chosun University, Gwangju 61452, Korea. ⁷These authors contributed equally: Duy Khuong Mai, Chanwoo Kim and Joomin Lee. ✉email: scho@chonnam.ac.kr; jaesung.yang@yonsei.ac.kr; hjkim@chosun.ac.kr

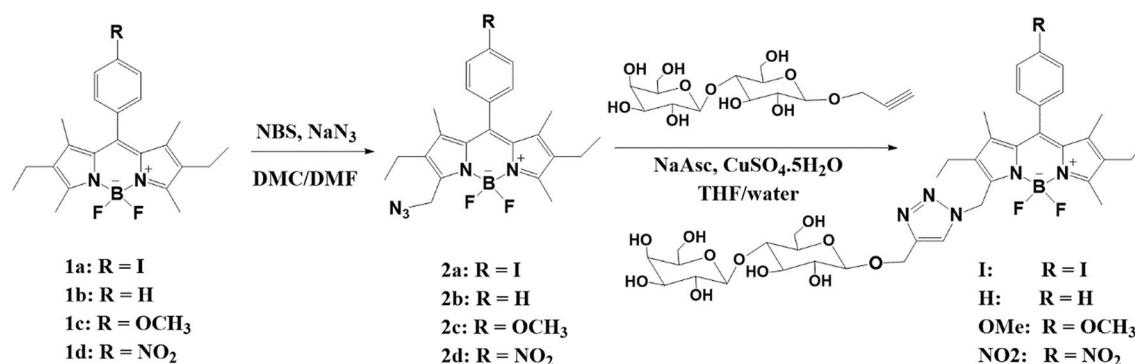


Figure 1. The preparation of lactose-functionalized BODIPY PSs with various *meso*-phenyl substituents.

Among the different PSs, 4, 4-difluoro-4-bora-3a,4a-diaza-s-indacene (BODIPY) is a new family of fluorescent dyes with outstanding photophysical features, such as high molar extinction coefficient, high quantum efficiencies of fluorescence, and easy electronic modification of frontier molecular orbitals by substituents. BODIPYs have thus been applied as promising imaging/detection agents with high light-to-dark toxicity ratios^{16–19}. Many dyes with a high ISC obtained from natural or synthetic sources have been employed in PDT reactions^{20,21}. The most common design strategy employed to enhance ISC efficiency is the conjugation of heavy halogen atoms (Br or I) to promote spin-orbit coupling (SOC), which improves the ¹O₂ generation capability and the population of longer-lived excited triplet states^{22,23}. However, the incorporation of heavy halogen atoms causes toxicity and fluorescence quenching^{24–26}. Therefore, BODIPY PSs without heavy halogen atoms are preferred as theranostic agents.

Several approaches with heavy-atom-free PSs to improve the ISC, such as the use of dimer BODIPY^{27,28}, spin converters²⁹, and photoinduced electron transfer (PeT)^{30,31}, have recently been reported. The formation of triplet states via photoinduced electron transfer (PeT) is a well-known process that was not employed to develop practical triplet sensitizers until recently³². The charge-transfer (CT) states comprised the donor radical cation and the acceptor radical anion are induced by PeT, which recombines the ground state via different pathways^{31,33,34}. Owing to the different polarity between locally-excited (LE) and CT states, their relative energy levels are strongly affected by the polarity of medium and accordingly the energy relaxation dynamics much complicated. For example, in non-polar solvents, the energy level of polar CT state is usually higher than that of the LE state, resulting in very low PeT efficiency and intense fluorescence from the LE state. In contrast, for solvents with sufficient polarity, such as in an aquatic environment, the CT state is energetically much stabilized and thus its energy level can be low lying compared to that of the LE state, causing effective PeT and ISC³⁵.

Recently, we reported a series of water-soluble BODIPY PSs attached to heavy atoms at the 2,6-position of the BODIPY core²⁴. These BODIPY PSs showed excellent PDT ability, while exhibiting very low dark toxicity; however, they could not be used as imaging reagents due to their low fluorescence quantum yield (Φ_F) resulting from the incorporation of heavy atoms. To overcome the above-mentioned issues, we aim to develop bifunctional heavy-atom-free BODIPY PSs with imaging-guided PDT properties. Herein, we present a new family of heavy-atom-free BODIPY nanoparticles (NPs) (Fig. 1) with potential applications in tumor-targeted fluorescence cell imaging and PDT. We synthesized four BODIPY PSs containing different substituent groups (-I, -H, -OCH₃, and -NO₂) in the *para*-phenyl moiety attached to the *meso*-position of the BODIPY core, and investigated their photophysical and photosensitizing properties according to the variation in the substituents. Among the BODIPY PSs, we used BODIPY **H** as an internal reference to compare the fluorescence and PDT efficiencies without substituent. In addition, BODIPY segments were connected with lactose-tethering triazole as a specific ligand for asialoglycoprotein (ASGP) in liver cancer cells³⁶. The resulting BODIPY PSs formed NPs with a uniform size in water. Further, the cell viability, cellular imaging, and photodynamic anticancer activities of these BODIPY NPs were evaluated using HeLa and Huh-7 cells. Overall, our findings indicate that BODIPY NPs are promising tumor-targeted PDT agents, with fluorescence cell imaging properties in live cancer cell lines.

Results and discussion

Synthesis and photophysical characterization of BODIPY NPs. The process used to synthesize the four BODIPY PSs (**I**, **H**, **OMe**, and **NO₂**) functionalized with lactose-tethering triazole is outlined in Fig. 1. The detailed procedure is provided in the Supporting Information section.

Compounds **1a–d** were synthesized via condensation reactions using 3-ethyl-2, 4-dimethyl pyrrole with 4-iodobenzoyl chloride and benzaldehyde derivatives, which yielded compounds **1a** and **1b–d**, respectively. Compounds **2a–d** modified with alkyl azide at the 3-methyl position of the BODIPY core were obtained in the same manner³⁷. Cu(I)-catalyzed alkyne-azide cycloaddition reactions (CuAAC) were performed with compounds **2a–d** and propargyl lactoside to obtain the final compounds BODIPY **I**, **H**, **OMe**, and **NO₂**, respectively. The final BODIPY PSs were fully characterized by ¹H, ¹³C NMR, and HR-MS, as shown in Fig. S8–27.

A series of water-dispersible NPs, namely **I-NPs**, **H-NPs**, **OMe-NPs**, and **NO₂-NPs**, were obtained from the corresponding BODIPY PSs **I**, **H**, **OMe**, and **NO₂** in aqueous solution, respectively, after complete evaporation of tetrahydrofuran (THF).

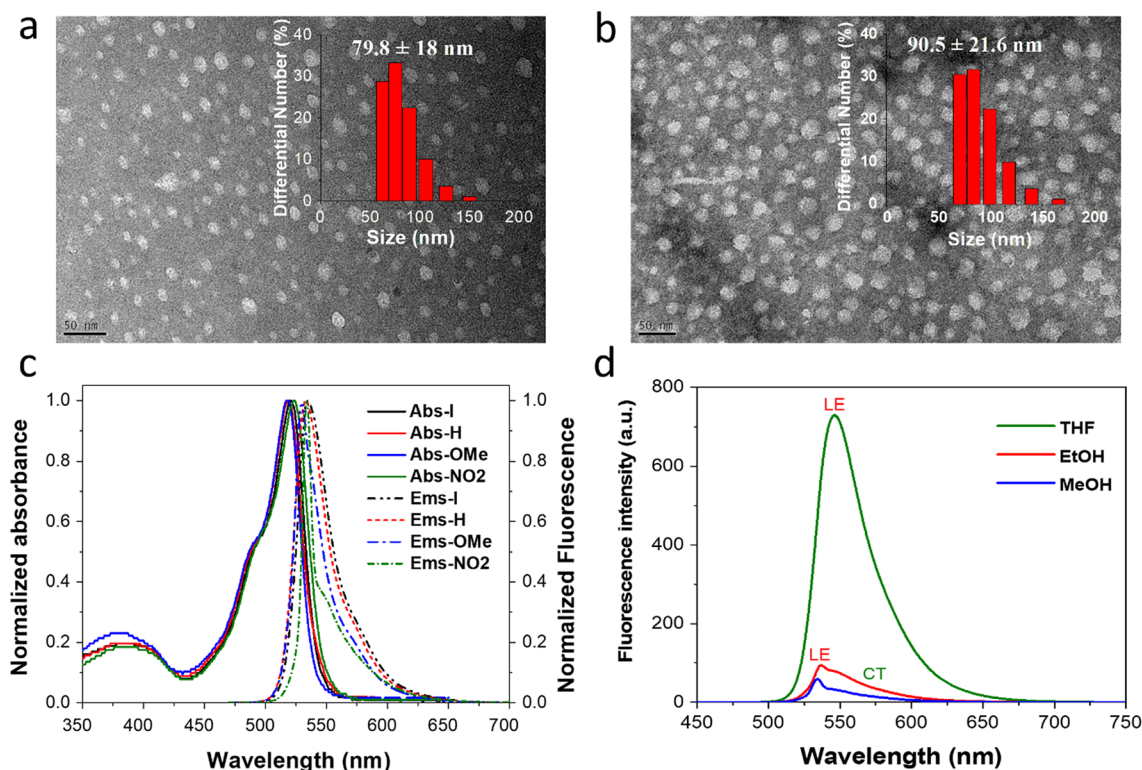


Figure 2. Characterization of BODIPY PSs. TEM images of **I-NPs** (a) and **OMe-NPs** (b) (the scale bar: 50 nm). The inset images indicate the sizes of **I-NPs** and **OMe-NPs** based on DLS. The normalized absorption and emission spectra of **I**, **H**, **OMe**, and **NO2** in methanolic solution at $c = 5 \mu\text{M}$ (c). The emission spectra of BODIPY **NO2** in various solvents at $c = 5 \mu\text{M}$ (d). The solutions were excited at 490 nm.

	I	H	OMe	NO₂
λ_{ab} (nm) ^a	522	518	520	524
λ_{em} (nm) ^a	535	533	530	534
ϵ ($10^3 \text{ M}^{-1} \text{ cm}^{-1}$) ^a	45.2	42.4	44.3	49.5
Φ_{F} ^b	0.45	0.51	0.49	0.014
Φ_{Δ} ^c	0.1	0.037	0.073	0.009

Table 1. The photophysical and photosensitizing properties of BODIPY **I**, **H**, **OMe**, and **NO2** in MeOH.

^aAbsorption and fluorescence data measured using methanol. ^bFluorescence quantum yields were determined using rhodamine 6G in methanol as the standard ($\Phi_{\text{F}} = 0.94$)⁴². ^cSinglet oxygen quantum yields were determined by the DPBF bleaching method, using HP in ethanol as a reference ($\Phi_{\Delta} = 0.53$)⁴³.

The hydrodynamic diameters of the obtained BODIPY NPs in aqueous solution were determined using dynamic light scattering (DLS) measurements. As shown in Fig. 2a,b and Figure S1, the average diameters of the **H**, **I**, **OMe**, and **NO2-NPs** were approximately 71.3, 79.8, 90.5, and 100.7 nm, respectively. The morphology and size of BODIPY NPs were also examined by transmission electron microscopy (TEM), which revealed their spherical morphology and average diameter of approximately 20–30 nm (Figs. 2a and b). Notably, the size of the fully hydrated BODIPY NPs as measured by DLS might be larger than that determined in the dried state from TEM. Many water molecules seem to be entrapped within the BODIPY NPs via interactions with hydrophilic lactose segments.

Figure 2c shows the absorption and fluorescence spectra of the BODIPY PSs in methanol. All of the synthesized BODIPY PSs exhibit typical two absorption bands, with a robust $S_0 \rightarrow S_1$ ($\pi \rightarrow \pi^*$) transition band around 518–524 nm, an extinction coefficient of 42,400–49,500 $\text{M}^{-1} \cdot \text{cm}^{-1}$ from the boradiazaindacene chromophore^{38,39}, and a weak broad band around 350–400 nm corresponding to the $S_0 \rightarrow S_2$ ($\pi \rightarrow \pi^*$) transition, which can be attributed to the out-of-plane vibrations of the aromatic skeleton^{37,40}. The iodine (-I) and methoxy (-OCH₃) substituents incorporated into the *meso*-phenyl of BODIPY resulted in almost the same absorption and emission spectra as BODIPY **H**, indicating that these substituents have a negligible effect on the photophysical properties of the BODIPY cores³⁷. The BODIPY dyes with **H**, **I**, and **OMe** exhibited a high Φ_{F} of approximately 0.45–0.51 (Table 1), which is usually recorded for BODIPY derivatives³⁷. Of note, the values of Φ_{F} remained high despite

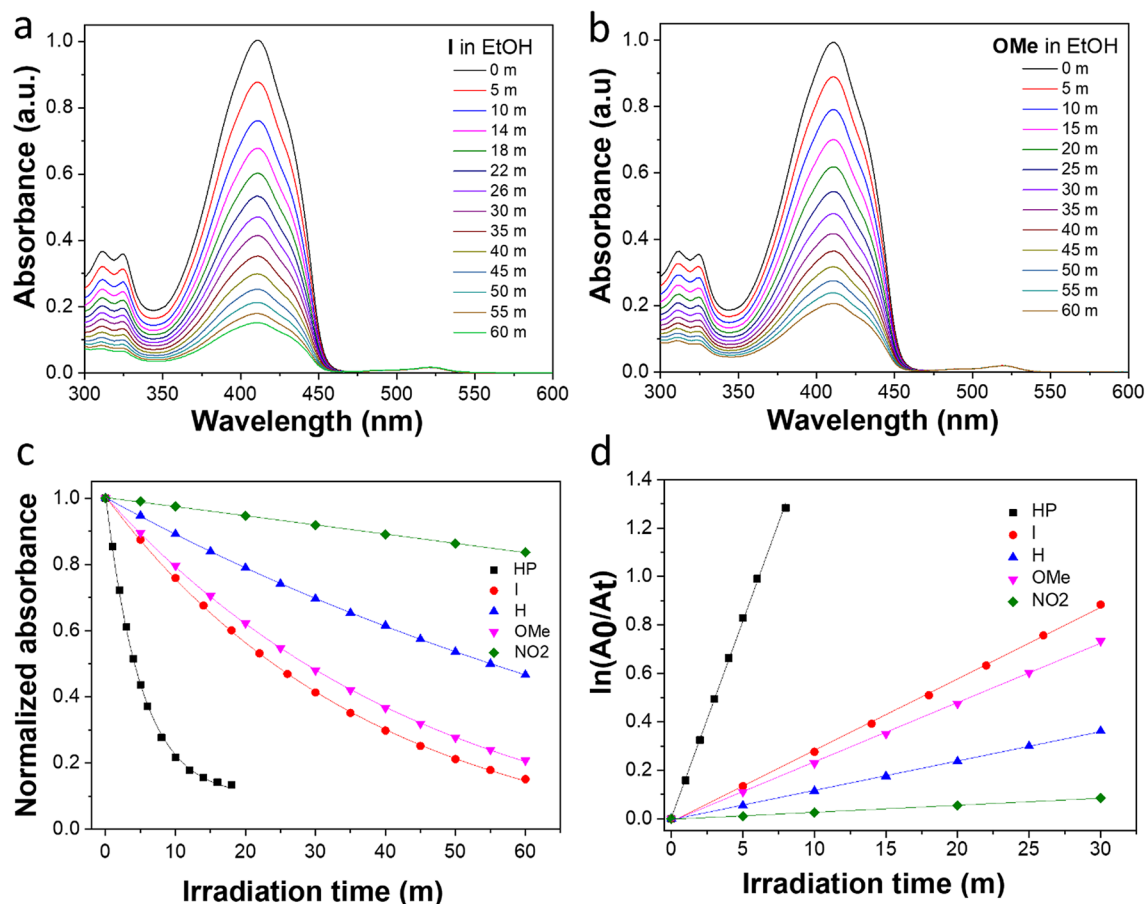


Figure 3. The singlet oxygen ($^1\text{O}_2$) generation capabilities of BODIPY PSs. Absorption spectra of DPBF upon irradiation in the presence of (a) **I** and (b) **OMe** under 520 nm for different times. (c) Plots of the change in absorbance of DPBF at 414 nm at different irradiation times using hematoporphyrin (HP) as the standard in EtOH at room temperature ($\Phi\Delta=0.53$). (d) $^1\text{O}_2$ assay using the absorbance attenuation of DPBF in the presence of BODIPY **I**, **H**, **OMe**, and **NO2** against HP as the standard in EtOH.

the BODIPY dyes being modified with the lactose-tethering triazole and iodine substituent^{24,41}. However, the nitro substituent ($-\text{NO}_2$) appeared to have a more significant influence on the photophysical properties of the BODIPY dye. Although the absorption spectrum of BODIPY **NO2** is similar to those of the other BODIPY PSs, its fluorescence quantum yield is largely reduced (Table 1) as well as its fluorescence intensity and spectral shape are strongly affected by the solvent polarity (Fig. 2d). In aqueous solution, BODIPY **I**, **H**, and **OMe**-NPs exhibited absorption and emission maxima ($\lambda_{\text{abs}}/\lambda_{\text{em}}$) at around 515/538 nm while the fluorescence of **NO2**-NPs was quenched (Figure S7).

As shown in Table S1, the emission intensities and Φ_{F} of **NO2** were largely quenched in protic polar solvents, exhibiting Φ_{F} of 0.035 in ethanol and 0.014 in methanol compared with 0.38 in THF. The intense emission observed in THF corresponds to the fluorescence from the local excited (LE) state of the BODIPY subunit. In contrast, fluorescence is largely quenched in a polar methanol solution, owing to a nearly non-emissive CT state⁴⁴. This phenomenon is expected because the population of non-emissive CT state by PeT mechanism competes with that of emissive LE state^{30,33,34}. Details of the photophysical studies are presented in the theoretical calculation section.

Singlet oxygen generation. The singlet oxygen ($^1\text{O}_2$) generation capabilities of **I**, **H**, **OMe**, and **NO2** were assessed in air-saturated ethanol under irradiation at 520 nm. A commercial $^1\text{O}_2$ probe, 1,3-diphenylisobenzofuran (DPBF), was used as an indicator, and hematoporphyrin (HP) in EtOH was used as the reference ($\Phi\Delta=0.53$)⁴⁵.

As shown in Figs. 3a–c and S3, the absorbance of DPBF at 414 nm decreased gradually in the presence of the BODIPY dyes under continuous light irradiation. According to the linear relationship of the decay curves (Fig. 3d), the $^1\text{O}_2$ quantum yields ($\Phi\Delta$) of **I**, **H**, **OMe**, and **NO2** were assigned as 0.1, 0.037, 0.073, and 0.009, respectively (Table 1). Thus, the most robust $^1\text{O}_2$ generation ability of **I** among the series of PS suggested that the additional heavy iodine atom on the *meso*-phenyl of BODIPY induced spin–orbit perturbations on the molecules and significantly influenced its superior capability to generate singlet oxygen, as shown by the faster reducing rate of DPBF absorbance bands and a higher $\Phi\Delta$ than that of the other BODIPY PSs. However, the incorporation of the electron-donating group ($-\text{OCH}_3$) at the *meso*-phenyl of BODIPY played an essential role

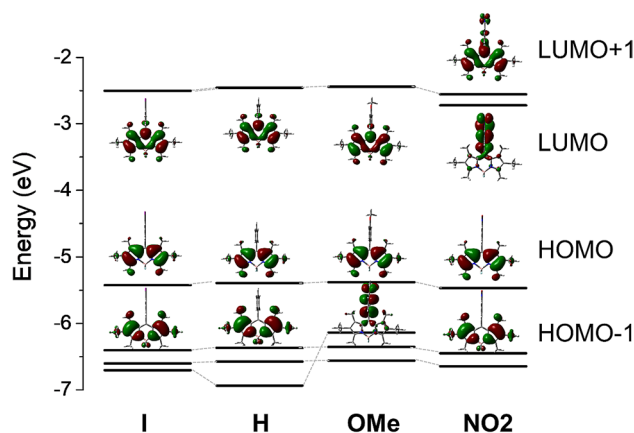


Figure 4. Energy diagram of frontier molecular orbitals of the BODIPY PSs.

in enhancing the $^1\text{O}_2$ generation of **OMe**. In contrast, the introduction of a strong electron-withdrawing group ($-\text{NO}_2$) did not lead to an efficient Φ_Δ of BODIPY **NO2** in a polar solvent (ethanolic solution). However, as shown in Figure S4a, Φ_Δ could be enhanced to 0.03 in a less polar solvent (THF). Such finding indicates that the triplet state of BODIPY **NO2** is strongly affected by the polarity of the media (the details are presented in the theoretical calculation). These results collectively indicate that both iodinated-*meso*-phenyl BODIPY **I** and heavy-free atom BODIPY **OMe** achieved an elevated $^1\text{O}_2$ under LED illumination that facilitated singlet oxygen generation, demonstrating their potential use as efficient photosensitizers for PDT.

Theoretical characterization of the BODIPY derivatives. To determine the effect of *meso*-phenyl substituents on the electronic structure of BODIPY PSs, density functional theory (DFT) calculations were performed (see Methods for computational details). As depicted in Fig. 4, the HOMO-3 of BODIPY **OMe** is destabilized by electron-donating methoxy substituent and consequently HOMO-1 of BODIPY **OMe** is mainly concentrated on methoxyphenyl (MPh). On the other hand, the LUMO of BODIPY **OMe** is fully concentrated on the BODIPY (BDP) moiety, implying that upon the generation of the singlet excited state by photoexcitation, PeT may occur, leading to the CT state, $^1[\text{BDP}^+-\text{MPh}^-]$. This process enhances the triplet state formation efficiency, as demonstrated by the significant increase in Φ_Δ of **OMe**, compared with **H**. The energy level of singlet CT state was approximately 0.2 eV higher in energy than that of the singlet excited state (Table S2). However, Filatov et al. suggested that even if the energy of the CT state is greater than that of the singlet excited state, PeT and the subsequent triplet state formation can occur, with a propensity that the efficiency of the processes reduces with increasing energy gap³⁰. Hence, despite the reversal of the state energy, PeT is viewed as a valid mechanism for **OMe**, which facilitates the generation of the triplet state and $^1\text{O}_2$.

The electron-withdrawing nitro group existing in **NO2** causes nitrophenyl (NPh) to act as an electron acceptor, while BODIPY becomes an electron donor, as demonstrated by the HOMO and LUMO localized on BODIPY and nitrophenyl, respectively (Figs. 4 and S5). Therefore, in **NO2**, PeT may produce $^1[\text{BDP}^+-\text{NPh}^-]$. Unlike **OMe**, the energy level of the CT state is much lower than that of the LE state of BODIPY moiety with an energy gap of 0.49 eV, and therefore the lowest CT state dominantly contributes to the energy relaxation after photoexcitation (Table S2). The results of the DFT calculations, in conjunction with the solvent dependency of Φ_F , clearly confirm the existence of PeT in **NO2**; however, this does not lead to efficient ISC and energy transfer to ground-state $^3\text{O}_2$, as reflected by the very low Φ_Δ of BODIPY **NO2**.

For donor-acceptor-type BODIPY dyads, comparing the frontier orbital energies of donor and acceptor units is beneficial for explaining electron movement during the PeT process⁴⁴. This approach applies to **NO2** because, in its optimized geometry, the two subunits are oriented almost perpendicular ($\theta_{\text{dihedral}} = 87.8^\circ$) and can be considered as two independent functional groups. In this context, to elucidate the unexpected decoupling between PeT and the triplet state formation observed for **NO2**, the HOMO/LUMO energies of hexaalkyl-substituted BODIPY and nitrobenzene were calculated and compared, shown in Fig. 5a.

As illustrated in Fig. 5b, ISC from $^1[\text{BDP}^+-\text{NPh}^-]$ to $^3[\text{BDP}^+-\text{MPh}]$ requires the back transfer of an electron from LUMO_{NPh} to LUMO_{BDP} following the conversion of its spin; this process is known as the radical pair ISC (RP-ISC). However, DFT calculations revealed that $E(\text{LUMO}_{\text{BDP}}) > E(\text{LUMO}_{\text{NPh}})$ (Fig. 5a), demonstrating that for **NO2**, back electron transfer (BeT) is an energetically unfavorable process. These findings agree with those of Zhao et al., who explored redox potentials for energetic comparison of frontier orbitals⁴⁶. In addition, electron spin conversion, which must precede the above process, is often forbidden for directly linked donor-acceptor systems, such as **NO2**. Hence, $^1[\text{BDP}^+-\text{NPh}^-]$ of **NO2** is most likely to decay nonradiatively to the ground state. However, whether this dissipation occurs directly or via the formation of $^3[\text{BDP}^+-\text{NPh}^-]$ remains unclear, but it is clear that even if the $^3[\text{BDP}^+-\text{NPh}^-]$ mainly formed, it does not contribute to the energy transfer to the ground-state $^3\text{O}_2$.

These results are consistent with those of Qi et al.⁴⁷ The electronic properties of the *meso*-substituent on the BODIPY core, particularly the introduction of a suitable electron-donating group, could be fine-tuned to control

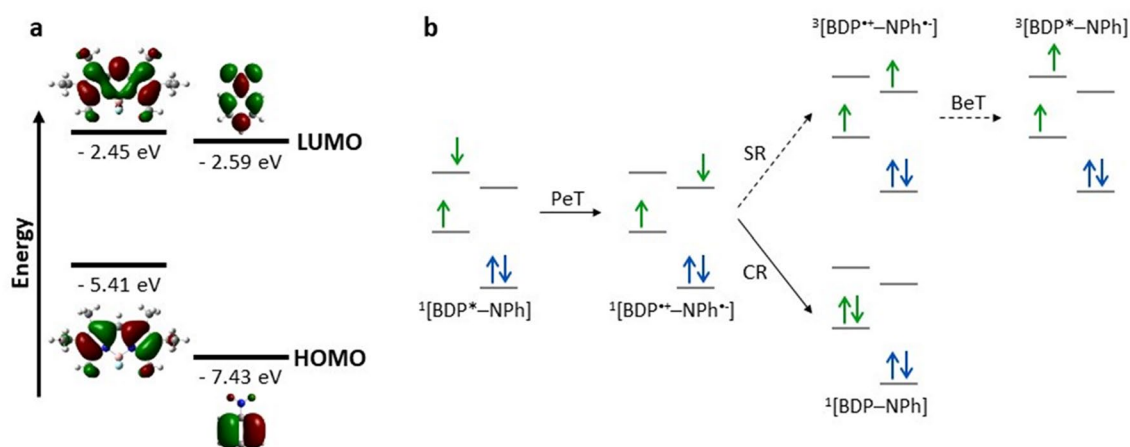


Figure 5. (a) Frontier orbital energies of two subunits of NO_2 . (b) Schematic of the electron movement required for PeT-mediated triplet state generation in NO_2 . In (b), SR, CR, and BeT represent spin reversion, charge recombination, and back electron transfer, respectively.

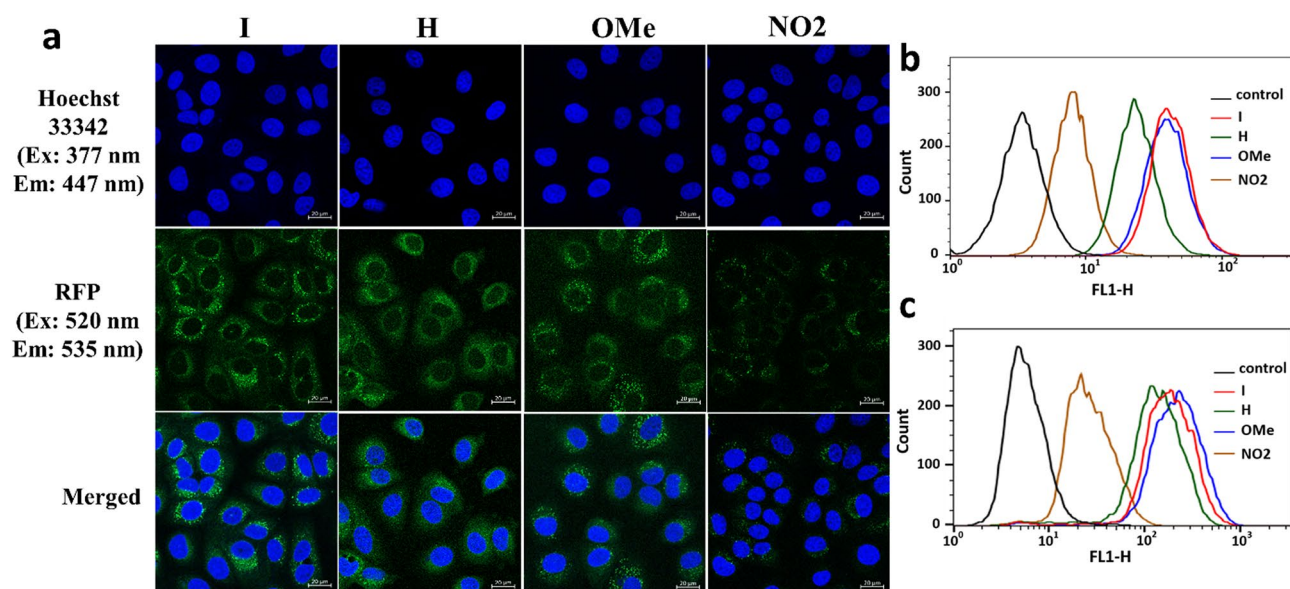


Figure 6. Cell selectivity and imaging of lactose-functionalized BODIPY PSs. Fluorescence images of Huh-7 cells were captured after a 2 h incubation with $2 \mu\text{M}$ of **I**, **H**, **OMe**, and **NO2**-NPs. After incubation, cell nuclei were stained with Hoechst 33,342 dye for 10 min. Images were captured with a $40\times$ objective lens and fluorescence optics (excitation at 520 nm for **I**, **H**, **OMe**, and **NO2**-NPs and 377 nm for Hoechst 33,342; and emission at 535 nm for **I**, **H**, **OMe**, and **NO2**-NPs and 447 nm for Hoechst 33,342). Scale bar = $20 \mu\text{m}$ (a). The fluorescence-activated cell sorting (FACS) analysis of HeLa (b) and Huh7 cells (c) treated with $2 \mu\text{M}$ of BODIPY **I**, **H**, **OMe**, and **NO2**. The incubation time was 2 h for all BODIPY NPs.

the efficiency of singlet oxygen formation. For BODIPY **I**, the perpendicular geometry between BODIPY and iodophenyl moieties prevents strong electronic coupling between BODIPY and iodine, and accordingly BODIPY **I** can maintain high fluorescence quantum yield despite the substitution of heavy-atom iodine. These results suggest that BODIPY **OMe** can be used as a theranostic agent for cancer treatment.

Cellular uptake and cell-imaging of BODIPY NPs. Cellular uptake behaviors of the BODIPY NPs against Huh-7 (human liver carcinoma) and HeLa (human cervix adenocarcinoma) cells were measured and compared by flow cytometry analysis. First, the cells were incubated with $2.0 \mu\text{M}$ of the BODIPY PSs for 2 h at 37°C ; then, the treated cells were collected and subjected to fluorescence-activated cell sorting (FACS). As depicted in Figs. 6b,c, these BODIPY NPs exhibited higher selectivity for Huh-7 cells than HeLa cells. The mean fluorescence of liver cancer cells treated with **I**, **H**, **OMe**, and **NO2**-NPs was approximately 4.6-, 6.2-, 6.1-, and fourfold higher than that of the treated HeLa cells (Fig. 6b,c and Table S3). Such finding is due to the high density of ASGP receptors on the surface of liver cancer cells, which can bind BODIPY NPs containing galactose

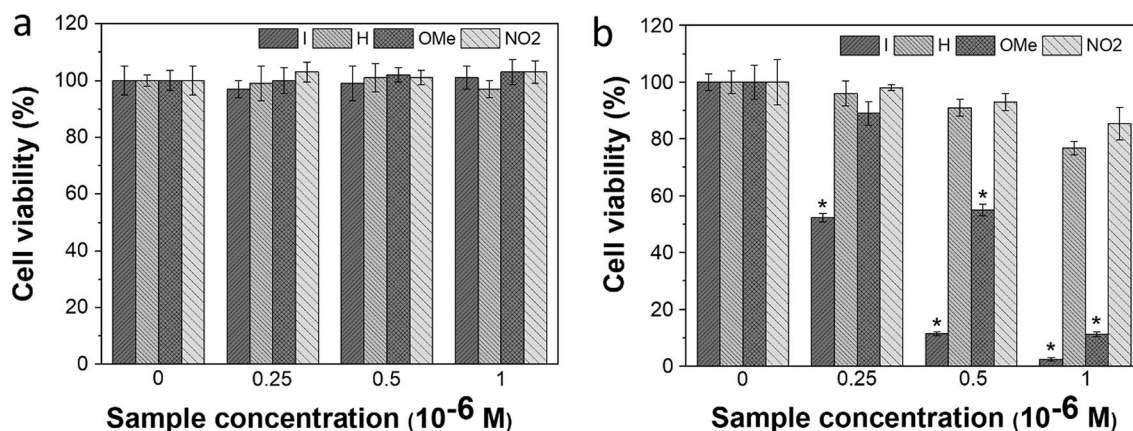


Figure 7. Photodynamic anticancer activities of BODIPY PSs in Huh-7 cells. Cytotoxicity (a) and phototoxicity (b) of BODIPY I, H, OMe, and NO₂-NPs in Huh-7 cells (hepatocellular carcinoma) under light irradiation (λ_{irr} 530 nm, 8.6 J·cm⁻²). The cell viabilities were detected using a CCK-8 kit after incubation with I, H, OMe, and NO₂-NPs for 24 h under dark conditions. Quantitative data are expressed as mean \pm standard deviation (n = 4). Statistical significance based on the Student's *t*-tests was considered as **p* < 0.05.

residues and be successfully internalized into Huh-7 cells via receptor recognition^{48,49}, which is consistent with our previous report²⁴. This result demonstrates that BODIPY PSs with versatile functional groups can have an improved targeting ability compared to imaging-guided PDT agents which cannot be chemically modified such as 5-aminolevulinic acid (ALA)⁵⁰.

Lactose modification can provide BODIPY NPs with potential applications in specific liver cancer imaging ability. To evaluate the potential application of the fluorescent dye for cell imaging, liver cancer Huh-7 cells were treated with these dyes for 2 h and imaged by confocal microscopy. Hoechst 33,342, a fluorescent stain commonly used to visualize the nucleus, was used to confirm fluorescent dye localization within the cells. As shown in the cellular images (Fig. 6a), the targeting BODIPY NPs could be effectively transported into Huh-7 cells, which was mediated by galactose receptors, after cultivation for 2 h and firmly gathered in the cytoplasm and perinuclear region. Hoechst 33,342 resulted in blue fluorescence in the nucleus of Huh-7 cells, and the merged image revealed that these BODIPY NPs could specifically bind to Huh-7 cells and localize in their cytoplasm. Therefore, these BODIPY NPs can effectively distinguish the cytoplasm of Huh-7 cells from the nucleus.

Huh-7 cells cultured with H, I, and OMe-NPs showed stronger fluorescence, whereas those cultured with NO₂-NPs displayed weaker fluorescence; this is caused by the high fluorescence of H, I, and OMe-NPs along with cellular uptake of NO₂-NPs being the lowest, consistent with the FACS results. Additionally, as mentioned above, NO₂-NPs exhibited PeT in polar media, resulting in the CT state, which inhibits fluorescence. As a result, NO₂-NPs appeared darker in the cell-imaging than the other compounds.

Light-induced cytotoxicity of BODIPY NPs against cancer cells. The biocompatibility of I, H, NO₂, and OMe-NPs with Huh-7 and HeLa cells was determined using MTS assays. As shown in Figs. 7a and S6a, there was no cytotoxicity in any of the tested cells, and more than 97% of both Huh-7 and HeLa cells survived after 24 h of incubation. Thus, all water-soluble BODIPY PSs below a dose of 1 μ M had good biocompatibility and did not induce severe cytotoxicity in fibroblasts and cancer cells, implying that BODIPY I, H, NO₂, and OMe-NPs could be used in the light cytotoxicity test.

For the efficient production of ROS, HeLa and Huh-7 cells were exposed to 530 nm laser irradiation at an extremely low energy of 8.6 J·cm⁻², and the in vitro phototoxicity of PDT was assessed. First, there was no significant variance when HeLa and Huh-7 cells were cultured with RPMI containing 1 μ M of H and NO₂-NPs, not only under dark conditions but also under irradiation; this is because of their low singlet oxygen quantum yield, as mentioned above. When exposed to LED light, I and OMe-NPs resulted in high phototoxicity to tumor cells and negligible cell toxicity in the dark, as shown in Figs. 7b and S6b. Cell viability evidently decreased as the concentration of these BODIPY NPs increased. Furthermore, when HeLa cells were exposed to light in the presence of 1 μ M of OMe and I-NPs, cell viability decreased by approximately 78% and 83%, respectively, while Huh-7 cells died by up to 89% and 97.7%, respectively, indicating their efficient PDT targeting ability. Besides, the half-lethal dose (IC₅₀) of OMe-NPs for HeLa and Huh-7 cell lines was 0.62 and 0.52 μ M, respectively. Notably, when exposed to light, the lactose-tethered BODIPY OMe and I-NPs killed more Huh-7 cells than HeLa cells, with IC₅₀ values of 0.51 and 0.26 μ M, respectively. These results demonstrate that BODIPY I and OMe-NPs provide better treatment efficacy with relatively low irradiation intensity than H and NO₂-NPs.

Conclusion. We designed and synthesized a series of lactose-functionalized BODIPY PSs with different substituent groups at the *meso*-position of the BODIPY core as cancer-targeted theragnostic agents for imaging and PDT. These BODIPY PSs could aggregate into nanoparticles (I-, H-, OMe-, and NO₂-NPs) in an aqueous solution and displayed a uniform size and shape, as determined by TEM and DLS. The fluorescence quantum yields of BODIPY I, H, and OMe were remarkably high, whereas that of BODIPY NO₂ was significantly lower

due to the PeT process in polar media. Among the four BODIPY photosensitizers, BODIPY **I** demonstrated high efficiency of singlet oxygen generation caused by the heavy atom effect due to the presence of an iodine atom, while BODIPY **OMe** containing an electron-donating methoxy group at the *meso*-phenyl moiety also enhanced the ISC efficiency. In contrast, the strong electron withdrawing by nitro group (NO₂) caused a marked reduction in both the fluorescence quantum yield and singlet oxygen formation efficiency of BODIPY **NO2** due to effective PeT in the polar media. The cellular experiments demonstrated that the water-soluble BODIPY NPs series showed good biocompatibility and cancer-specific fluorescence imaging ability. Notably, BODIPY **OMe** and **I**-NPs presented excellent phototoxicity against cancer cells, especially, liver cancer Huh-7 cells. The biocompatible BODIPY NPs have proven to be promising for developing highly efficient theragnostic agents for imaging-guided PDT for cancer treatment.

Methods

Materials instrumentations. Almost all reagents and chemicals were obtained from Sigma Aldrich (St. Louis, MO, USA). Some solvents such as dichloromethane (CH₂Cl₂), methanol (MeOH), or MgSO₄, sodium azide (NaN₃), sodium ascorbate (NaAsc), Copper (II) sulfate pentahydrate (CuSO₄·5H₂O) were purchased from Daejung chemical (Gyeonggi-do, South Korea), and used without further purification. Lactose-propargyl was synthesized in our previous literature²⁴.

All compounds were characterized by ¹H and ¹³C-NMR spectroscopy on a Bruker AM 250 spectrometer (Billerica, MA, USA). The impurity of the products was checked by thin-layer chromatography (TLC, silica gel 60 mesh). UV spectra were measured on a Shimadzu UV-1650PC spectrometer, and fluorescence spectra were carried on a Hitachi F-7000 spectrometer. The size and morphology of BODIPY NPs were analyzed by using dynamic light scattering (DLS) on Malvern Zetasizer Nano ZS90 and transmission electron microscopy (TEM). We used machine JEOL- JEM 2100F at an accelerating voltage of 200 kV. The sample for TEM was prepared according to our reported literature⁵¹.

Synthesize of water-soluble BODIPY **I, **H**, **OMe**, and **NO2**:** According to our reported literature²⁴, the series of water-soluble BODIPY **I**, **H**, **OMe**, and **NO2** were prepared using the same pathway. A representative routine is presented for the compound **I**. Briefly, BODIPY **2a** (80 mg, 0.157 mmol), lactose propargyl (66 mg, 0.173 mmol), NaAsc (156 mg, 0.785 mol), and CuSO₄·5H₂O (79 mg, 0.316 mmol) were dissolved in the mixture of THF/water (15/5 mL, v/v). The resulting mixture was stirred for one day at room temperature, extracted with THF and water three times, and dried over MgSO₄. After removing the solvent by a rotary evaporator, the crude product was purified by recrystallization using MeOH/diethyl ether to afford an orange solid (yield 76 mg, 52% yield). ¹H NMR (300 MHz, CD₃OD, δ, ppm): δ 8.02 (s, 1H), 7.97- 7.95 (d, 2H), 7.17- 7.15 (d, 2H), 5.83 (s, 2H), 4.36- 4.33 (d, 2H), 3.87- 3.85 (d, 2H), 3.81- 3.80 (d, 2H), 3.76- 3.74 (d, 1H), 3.71- 3.69 (d, 1H), 3.57- 3.53 (d, 2H), 3.49- 3.48 (d, 2H), 3.31- 3.29 (d, 2H), 2.57 (s, 3H), 2.42-2.39 (q, 4H), 1.44 (s, 3H), 1.36 (s, 3H), 1.28 (s, 3H), 1.05- 1.00 (t, 3H). ¹³C NMR (75 MHz, CD₃OD, δ, ppm): δ 162.25, 143.55, 143.24, 142.81, 140.13, 138.60, 137.3, 135.75, 134.58, 134.16, 131.48, 131.32, 105.09, 103.29, 96.18, 80.57, 77.05, 76.45, 76.29, 74.75, 74.58, 72.52, 70.38, 63.00, 62.42, 61.82, 46.12, 17.57, 17.32, 14.87, 14.76, 13.2, 12.45, 11.92. HRMS (ESI): calculated for (C₃₈H₄₉BF₂IN₅O₁₁): m/z: [M]: 928.2613; found: 928.2619.

Compound **H:** BODIPY **H** was synthesized according to the general procedure to afford the orange solid (67 mg, 57% yield). ¹H NMR (300 MHz, CD₃OD, δ, ppm): δ 8.01 (s, 1H), 7.59- 7.57 (t, 3H), 7.37- 7.36 (d, 2H), 5.84 (s, 2H), 4.37- 4.33 (d, 2H), 3.87- 3.85 (d, 2H), 3.81- 3.80 (d, 2H), 3.76- 3.73 (d, 1H), 3.69- 3.66 (d, 1H), 3.59- 3.57 (d, 2H), 3.54- 3.52 (d, 2H), 3.49- 3.32 (d, 2H), 2.53 (s, 3H), 2.43-2.38 (q, 4H), 1.38 (s, 3H), 1.31 (s, 3H), 1.28 (s, 3H), 1.04- 0.99 (t, 3H). ¹³C NMR (75 MHz, CD₃OD, δ, ppm): δ 161.82, 144.19, 143.61, 143.46, 138.71, 136.45, 134.29, 131.7, 130.75, 130.61, 129.43, 105.16, 103.36, 80.45, 77.26, 77.15, 76.41, 74.6, 72.4, 70.26, 62.96, 62.53, 61.77, 61.66, 48.07, 17.68, 14.85, 14.5, 13.16, 12.24, 11.66. HRMS (ESI): calculated for (C₃₈H₅₅BF₂IN₅O₁₂Na): m/z: [M + Na]⁺: 834.3713; found: 834.3714.

Compound **OMe:** BODIPY **OMe** was synthesized according to the general procedure to afford the orange solid (55 mg, 47% yield). ¹H NMR (300 MHz, CD₃OD, δ, ppm): δ 8.0 (s, 1H), 7.23- 7.2 (d, 2H), 7.13- 7.1 (d, 2H), 5.87 (s, 2H), 4.37- 4.34 (d, 2H), 3.89 (s, 3H), 3.77- 3.71 (q, 3H), 3.6- 3.5 (m, 6H), 3.42- 3.39 (d, 1H), 2.56 (s, 3H), 2.4-2.38 (q, 4H), 1.43 (s, 3H), 1.36 (s, 3H), 1.28 (s, 3H), 1.01- 0.95 (t, 3H). ¹³C NMR (75 MHz, CD₃OD, δ, ppm): δ 162.15, 144.48, 143.03, 138.59, 136.87, 134.71, 134.18, 132.17, 130.55, 128.29, 116.06, 105.04, 103.33, 80.37, 77.08, 76.53, 76.22, 74.82, 74.64, 72.64, 70.21, 63.04, 62.43, 61.75, 55.8, 46.14, 17.73, 17.44, 14.87, 14.26, 13.28, 12.53, 11.56. HRMS (ESI): calculated for (C₃₉H₅₂BF₂N₅O₁₂Na): m/z: [M + Na]⁺: 854.3571; found: 854.3572.

Compound **NO2:** BODIPY **NO2** was synthesized according to the general procedure to afford the orange solid (80 mg, 61% yield). ¹H NMR (300 MHz, CD₃OD, δ, ppm): δ 8.47- 8.44 (d, 2H), 8.01 (s, 1H), 7.69- 7.66 (d, 2H), 5.83 (s, 2H), 4.37- 4.34 (d, 2H), 3.86- 3.32 (d, 2H), 3.79- 3.75 (d, 2H), 3.6- 3.5 (m, 6H), 3.31- 3.29 (d, 2H), 2.59 (s, 3H), 2.41- 2.39 (q, 4H), 1.39 (s, 3H), 1.31 (s, 3H), 1.29 (s, 3H), 1.04- 0.98 (t, 3H). ¹³C NMR (75 MHz, CD₃OD, δ, ppm): δ 163.11, 149.96, 143.16, 141.37, 138.46, 137.78, 134.63, 133.69, 131.64, 130.96, 125.76, 105.14, 103.6, 80.37, 77.35, 76.4, 76.24, 74.84, 74.35, 72.54, 70.36, 63.11, 62.44, 61.76, 46.06, 19.39, 17.86, 14.86, 14.46, 13.09, 12.63, 11.71. HRMS (ESI): calculated for (C₃₈H₄₉BF₂N₆O₁₃Na): m/z: [M + Na]⁺: 869.3316; found: 869.3318.

Measurement of photophysical properties. The Φ_f were measured by a comparative method using the standard reference with the already-known value of Φ_f as the following Eq. (1):

$$\Phi_S = \Phi_R \left(\frac{A_R}{A_S} \right) \left(\frac{n_S}{n_R} \right)^2 \left(\frac{D_S}{D_R} \right) \quad (1)$$

The subscript of S and R represent sample and reference, respectively. N is the refractive index of solvent. A and D are the absorbance and the integrated fluorescence area, respectively. Solutions should be optically dilute to avoid inner filter effects. The Rhodamine 6G was used as the reference sample, which possessed a known quantum yield of 0.94⁴².

Detection of singlet oxygen quantum yields. The quantum yields of singlet oxygen (Φ_{Δ}) of BODIPY **I**, **H**, **OMe**, and **NO2** were studied using diphenylisobenzofuran (DBPF) as a chemical quencher⁴³. Briefly, a mixture of the BODIPY dye (absorption ~ 0.02 at 520 nm in EtOH) and the DPBF (absorption ~ 1.0 at 414 nm in EtOH) was irradiated with a laser light ($\lambda_{irr} = 520$ nm). The photooxidation of DPBF was monitored between 0–60 min depending on the efficiency of the PSs. The singlet oxygen quantum yield was calculated using hematoporphyrin (HP) as the reference with a yield of 0.53 in ethanol according to the following Eq. (2):

$$\Phi_{\Delta}^S = \Phi_{\Delta}^R \times \frac{k_S}{k_R} \times \frac{F_R}{F_S} \quad (2)$$

where Φ_{Δ}^R is the singlet oxygen quantum yield of the reference, k is the slope of the photodegradation rate of DPBF, S means the sample, R represents the reference. F denotes the absorption correction factor, given by $F = 1 - 10^{-OD}$ (OD at the irradiation wavelength).

Quantum chemical calculations. Molecular structure optimizations for BODIPY derivatives were carried out using density functional theory (DFT), and their electronic states were calculated using time-dependent DFT (TD-DFT). For **H**, **OMe**, and **NO2**, the b3lyp functional of the Gaussian 16 program package and 6-31G(d) basis sets were chosen. For **I**, due to the heavy iodine atom, lanl2dz basis sets were chosen instead. All calculations were carried out in water solvent environment. The lactose-tethered triazole moiety attached to the position of the BODIPY core was confirmed to have a negligible influence on calculation results (Figure S2) and therefore was replaced by a hydrogen atom for simplicity.

Preparation of BODIPY nanoparticles (NPs). The stock solution of each BODIPY dyes in THF (0.5 mg. ml⁻¹) was prepared, then 50 μ L of stock solution was slowly added to 5 mL of water. The mixture was stirred overnight to evaporate all of THF naturally to yield the designed nanoparticles for further experiment.

Cells and cell culture. HeLa (human cervix adenocarcinoma), Huh7 (human liver carcinoma) cells were obtained from the Korean Cell Line Bank. The cells were maintained in RPMI 1640 medium (Gibco, Carlsbad, CA, USA) supplemented with 10% heat-inactivated fetal bovine serum (FBS) and antibiotics (100 U/mL penicillin and 100 mg/mL streptomycin) at 37 °C in a humidified 5% CO₂ incubator.

Cell proliferation assay. Cell proliferation was studied using CellTiter 96[®] Aqueous One Solution Cell Proliferation Assay (Promega, Madison, WI, USA) according to the manufacturer's instructions. Briefly, HeLa and Huh7 (3 $\times 10^3$ cells/well) were seeded in 96-well plates. After the cells were maintained for 24 h, cells were treated with BODIPY **I**, **H**, **OMe**, and **NO2** at different concentrations (0, 0.25, 0.5, and 1 μ M) for 24 h. Following 24 h of incubation, 20 μ L MTS [3-(4, 5-dimethylthiazol-2-yl)-5-(3-carboxymethoxyphenyl)-2-(4-sulfophenyl)-2H-tetrazolium] reagent were added to each well and incubated for 4 h at 37 °C. The absorbance was determined at 490 nm using an ELISA plate reader (Thermo Fisher Scientific, Inc., Waltham, MA, USA).

Assessment of cellular uptake and cellular imaging. To confirm the cellular uptake and cellular imaging by using the BODIPY **I**, **H**, **OMe**, and **NO2**, Huh-7 cells were incubated with 2 μ M of BODIPY **I**, **H**, **OMe**, and **NO2** for 2 h and washed three times with DPBS. After then, the cells were subsequently counterstained with Hoechst 33,342 for 10 min. After washing three times with DPBS, the morphologies of Huh-7 cells were taken by an automated live-cell imager (Lionheart FX, BioTek Instruments, Inc., VT, USA) with 40 \times objective lens and fluorescence optics (excitation at 520 nm for BODIPY **I**, **H**, **OMe**, and **NO2** and at 377 nm for Hoechst 33,342, and emission at 535 nm for BODIPY **I**, **H**, **OMe**, and **NO2** and at 447 nm for Hoechst 33,342). Cellular images were analyzed using Gen5[™] imager software (Ver.3.04, BioTek Instruments, Inc., VT, USA).

Photodynamic anticancer activity assessment. The HeLa and Huh7 cells were seeded at 3 $\times 10^3$ cells/well in a 96-well plate and incubated at 37 °C in 5% CO₂. After 24 h, the cells were incubated again with various concentrations of BODIPY **I**, **H**, **OMe**, and **NO2** (0, 0.25, 0.5, and 1 μ M) at 37 °C in 5% CO₂ for 2 h under dark conditions. After 2 h incubation for uptaking the BODIPY **I**, **H**, **OMe**, and **NO2** into the cells, the media in all plates were changed with RPMI 1640 media without phenol red. Irradiation of cells was performed with a green light-emitting diode (LED) using about 9 mW (530 nm, for 20 min, 80%). After irradiation, the cells were incubated for an additional 24 h, and the cell proliferation was measured using CellTiter 96[®] Aqueous One Solution Cell Proliferation Assay as the same method for the cytotoxicity described above.

Cellular uptake using flow cytometry. The cells (HeLa and Huh7) were seeded at 1 $\times 10^5$ cells/well in 6-well plate. After 24 h incubation at 37 °C in 5% CO₂, the BODIPY **I**, **H**, **OMe**, and **NO2** (2 μ M) were treated with cells for 2 h. Then, the cell were washed with phosphate buffered saline and analyzed using flow cytometry FC500 (Beckman coulter, CA, USA).

Statistical analysis

All results are expressed as the means \pm standard deviations and were compared by one-way analysis of variance (ANOVA followed by Tukey's analysis with Prism GraphPad 6 software (San Diego, CA, USA). A significance level was set at $*p < 0.05$.

Received: 21 August 2021; Accepted: 19 January 2022

Published online: 15 February 2022

References

- Allison, R. R. & Sibata, C. H. Oncologic photodynamic therapy photosensitizers: a clinical review. *Photodiagn. Photodyn. Ther.* **7**, 61–75 (2010).
- Baskaran, R., Lee, J. & Yang, S.-G. Clinical development of photodynamic agents and therapeutic applications. *Biomater. Res.* **22**, 1–8 (2018).
- Li, X., Lovell, J. F., Yoon, J. & Chen, X. Clinical development and potential of photothermal and photodynamic therapies for cancer. *Nat. Rev. Clin. Oncol.* **17**, 657–674 (2020).
- Kwiatkowski, S. *et al.* Photodynamic therapy—mechanisms, photosensitizers and combinations. *Biomed. Pharmacother.* **106**, 1098–1107 (2018).
- Mansoori, B. *et al.* Photodynamic therapy for cancer: Role of natural products. *Photodiagn. Photodyn. Ther.* **26**, 395–404 (2019).
- Benov, L. Photodynamic therapy: current status and future directions. *Med. Princ. Pract.* **24**, 14–28 (2015).
- dos Santos, A. I. F., de Almeida, D. R. Q., Terra, L. F., Baptista, M. c. S. & Labriola, L. Photodynamic therapy in cancer treatment—an update review. *J. Cancer Metast. Treatment* **5** (2019).
- Li, L. *et al.* Interaction and oxidative damage of DVDMS to BSA: a study on the mechanism of photodynamic therapy-induced cell death. *Sci. Rep.* **7**, 1–11 (2017).
- Naidoo, C., Kruger, C. A. & Abrahamse, H. Photodynamic therapy for metastatic melanoma treatment: A review. *Technol. Cancer Res. Treat.* **17**, 1533033818791795 (2018).
- Civantos, F. J. *et al.* A review of photodynamic therapy for neoplasms of the head and neck. *Adv. Ther.* **35**, 324–340 (2018).
- Kumar, R. *et al.* Small conjugate-based theranostic agents: an encouraging approach for cancer therapy. *Chem. Soc. Rev.* **44**, 6670–6683 (2015).
- Sirotkina, M. *et al.* Photodynamic therapy monitoring with optical coherence angiography. *Sci. Rep.* **7**, 1–11 (2017).
- Wang, C. *et al.* Microenvironment-triggered dual-activation of a photosensitizer-fluorophore conjugate for tumor specific imaging and photodynamic therapy. *Sci. Rep.* **10**, 1–9 (2020).
- Cai, Y. *et al.* Organic dye based nanoparticles for cancer phototheranostics. *Small* **14**, 1704247 (2018).
- Lan, M. *et al.* Photosensitizers for photodynamic therapy. *Adv. Healthcare Mater.* **8**, 1900132 (2019).
- Bui, H. T. *et al.* Effect of substituents on the photophysical properties and bioimaging application of BODIPY derivatives with triphenylamine substituents. *J. Phys. Chem. B* **123**, 5601–5607 (2019).
- Guo, Z. *et al.* Bifunctional platinumed nanoparticles for photoinduced tumor ablation. *Adv. Mater.* **28**, 10155–10164 (2016).
- Nguyen, V.-N. *et al.* Recent developments of BODIPY-based colorimetric and fluorescent probes for the detection of reactive oxygen/nitrogen species and cancer diagnosis. *Coordinat. Chem. Rev.* **439**, 213936 (2021).
- Zhang, T., Ma, C., Sun, T. & Xie, Z. Unadulterated BODIPY nanoparticles for biomedical applications. *Coord. Chem. Rev.* **390**, 76–85 (2019).
- Plaetzer, K., Krammer, B., Berlanda, J., Berr, F. & Kiesslich, T. Photophysics and photochemistry of photodynamic therapy: fundamental aspects. *Lasers Med. Sci.* **24**, 259–268 (2009).
- Kim, B. *et al.* In vitro photodynamic studies of a BODIPY-based photosensitizer. *Eur. J. Org. Chem.* **2017**, 25–28 (2016).
- Zou, J. *et al.* BODIPY derivatives for photodynamic therapy: influence of configuration versus heavy atom effect. *ACS Appl. Mater. Interfaces* **9**, 32475–32481 (2017).
- Wang, Z. *et al.* BODIPY-doped silica nanoparticles with reduced dye leakage and enhanced singlet oxygen generation. *Sci. Rep.* **5**, 12602 (2015).
- Khuong Mai, D. *et al.* Synthesis and photophysical properties of tumor-targeted water-soluble BODIPY photosensitizers for photodynamic therapy. *Molecules* **25** (2020).
- Aoife Gorman, J. K., O'Shea, C., Kenna, T., Gallagher, W. M. & O'Shea, D. F. In vitro demonstration of the heavy-atom effect for photodynamic therapy. *J. Am. Chem. Soc.* **126**, 10619–10631 (2004).
- Takatoshi-Yogo, Y. U., Ishitsuka, Y., Maniwa, F. & Nagano, T. Highly efficient and photostable photosensitizer based on BODIPY chromophore. *J. Am. Chem. Soc.* **127**, 12162–12163 (2005).
- Lu, S. *et al.* PEGylated dimeric BODIPY photosensitizers as nanocarriers for combined chemotherapy and cathepsin B-activated photodynamic therapy in 3D tumor spheroids. *ACS Appl. Bio Mater.* **3**, 3835–3845 (2020).
- Chen, H., Bi, Q., Yao, Y. & Tan, N. Dimeric BODIPY-loaded liposomes for dual hypoxia marker imaging and activatable photodynamic therapy against tumors. *J. Mater. Chem. B* **6**, 4351–4359 (2018).
- Ucuncu, M. *et al.* BODIPY-Au(I): A photosensitizer for singlet oxygen generation and photodynamic therapy. *Org. Lett.* **19**, 2522–2525 (2017).
- Filatov, M. A. *et al.* Control of triplet state generation in heavy atom-free BODIPY-anthracene dyads by media polarity and structural factors. *Phys. Chem. Chem. Phys.* **20**, 8016–8031 (2018).
- Callaghan, S., Filatov, M. A., Savoie, H., Boyle, R. W. & Senge, M. O. In vitro cytotoxicity of a library of BODIPY-anthracene and -pyrene dyads for application in photodynamic therapy. *Photochem. Photobiol. Sci.* **18**, 495–504 (2019).
- Filatov, M. A. Heavy-atom-free BODIPY photosensitizers with intersystem crossing mediated by intramolecular photoinduced electron transfer. *Org. Biomol. Chem.* **18**, 10–27 (2019).
- Lingling-Li, J. H., Nguyen, B. & Burgess, K. Syntheses and spectral properties of functionalized, water-soluble BODIPY derivatives. *J. Org. Chem.* **73**, 1963–1970 (2008).
- Dorh, N. *et al.* BODIPY-based fluorescent probes for sensing protein surface-hydrophobicity. *Sci. Rep.* **5**, 18337 (2015).
- Hisato Sunahara, Y. U., Kojima, H. & Nagano, T. Design and synthesis of a library of BODIPY-based environmental polarity sensors utilizing photoinduced electron-transfer-controlled fluorescence ON/OFF switching. *J. Am. Chem. Soc.* **129**, 5597–5604 (2007).
- Kim, T. H., Park, I. K., Nah, J. W., Choi, Y. J. & Cho, C. S. Galactosylated chitosan/DNA nanoparticles prepared using water-soluble chitosan as a gene carrier. *Biomaterials* **25**, 3783–3792 (2004).
- Ulrich, G., Ziesel, R. & Haefele, A. A general synthetic route to 3,5-substituted boron dipyrromethenes: applications and properties. *J. Org. Chem.* **77**, 4298–4311 (2012).
- Shilei Zhu, J. Z., Vegesna, G., Luo, F. T., Green, S. A. & Liu, H. Highly water-soluble neutral BODIPY dyes with controllable fluorescence quantum yields. *Org. Lett.* **13**, 438–441 (2011).

39. Vu, T. T. *et al.* Understanding the spectroscopic properties and aggregation process of a new emitting boron dipyrromethene (BODIPY). *J. Phys. Chem. C* **117**, 5373–5385. <https://doi.org/10.1021/jp3097555> (2013).
40. Sun, H. *et al.* Excellent BODIPY dye containing dimethylboryl groups as PeT-based fluorescent probes for fluoride. *J. Phys. Chem. C* **115**, 19947–19954 (2011).
41. Papalia, T. *et al.* Cell internalization of BODIPY-based fluorescent dyes bearing carbohydrate residues. *Dyes Pigm.* **110**, 67–71 (2014).
42. Douglas-Magde, R. W. A. P. G. S. Fluorescence quantum yields and their relation to lifetimes of rhodamine 6G and fluorescein in nine solvents: improved absolute standards for quantum yields. *Photochem. Photobiol.* **75**(4), 327–334 (2002).
43. Wolfgang-Spiller, H. K., Woehrl, D., Hackbarth, S., Roder, B. & Schnurpfeil, G. Singlet oxygen quantum yields of different photosensitizers in polar solvents and micellar solutions. *J. Porphyr. Phthalocyan.* **2**, 145–158 (1998).
44. Filatov, M. A. *et al.* Generation of triplet excited states via photoinduced electron transfer in meso-anthra-BODIPY: fluorogenic response toward singlet oxygen in solution and in vitro. *J. Am. Chem. Soc.* **139**, 6282–6285 (2017).
45. Liane M. Rossi, P. R. S., Vono, L. L. R., Fernandes, A. U., Tada, D. B., & Baptista M.S. Protoporphyrin IX nanoparticle carrier: preparation, optical properties, and singlet oxygen generation. *Langmuir* **24**, 12534–12538 (2008).
46. Hu, W. *et al.* Can BODIPY-electron acceptor conjugates act as heavy atom-free excited triplet state and singlet oxygen photosensitizers via photoinduced charge separation-charge recombination mechanism? *J. Phys. Chem. C* **123**, 15944–15955 (2019).
47. Qi, S., Kwon, N., Yim, Y., Nguyen, V. N. & Yoon, J. Fine-tuning the electronic structure of heavy-atom-free BODIPY photosensitizers for fluorescence imaging and mitochondria-targeted photodynamic therapy. *Chem. Sci.* **11**, 6479–6484 (2020).
48. Lu, Z. *et al.* Water-soluble BODIPY-conjugated glycopolymers as fluorescent probes for live cell imaging. *Polym. Chem.* **4** (2013).
49. Liu, L., Ruan, Z., Li, T., Yuan, P. & Yan, L. Near infrared imaging-guided photodynamic therapy under an extremely low energy of light by galactose targeted amphiphilic polypeptide micelle encapsulating BODIPY-Br 2. *Biomater Sci* **4**, 1638–1645 (2016).
50. Sando, Y. *et al.* 5-aminolevulinic acid-mediated photodynamic therapy can target aggressive adult T cell leukemia/lymphoma resistant to conventional chemotherapy. *Sci. Rep.* **10**, 1–11 (2020).
51. Khuong Mai, D. *et al.* Aggregation-induced emission of tetraphenylethene-conjugated phenanthrene derivatives and their bio-imaging applications. *Nanomaterials (Basel)* **8** (2018).

Acknowledgements

This work was performed with financial support from the research funds provided by Chosun University in 2021.

Author contributions

D.K.M., H.J.K. designed the protocol. D.K.M., I.W.B., and T.P.V. carried out the experiments. J.L. conducted cell experiments. C.K. studied computational modeling work. S.C., J.Y., and H.J.K. supported and advised the experiments. D.K.M., J.Y., and H.J.K. wrote the manuscript. All authors discussed the results and commented on the manuscript.

Competing interests

The authors declare no competing interests.


Additional information

Supplementary Information The online version contains supplementary material available at <https://doi.org/10.1038/s41598-022-06000-5>.

Correspondence and requests for materials should be addressed to S.C., J.Y. or H.-J.K.

Reprints and permissions information is available at www.nature.com/reprints.

Publisher's note Springer Nature remains neutral with regard to jurisdictional claims in published maps and institutional affiliations.

 **Open Access** This article is licensed under a Creative Commons Attribution 4.0 International License, which permits use, sharing, adaptation, distribution and reproduction in any medium or format, as long as you give appropriate credit to the original author(s) and the source, provide a link to the Creative Commons licence, and indicate if changes were made. The images or other third party material in this article are included in the article's Creative Commons licence, unless indicated otherwise in a credit line to the material. If material is not included in the article's Creative Commons licence and your intended use is not permitted by statutory regulation or exceeds the permitted use, you will need to obtain permission directly from the copyright holder. To view a copy of this licence, visit <http://creativecommons.org/licenses/by/4.0/>.

© The Author(s) 2022